

Focal Sweep Imaging with Multi-focal Diffractive Optics

Yifan Peng^{2,3} Xiong Dun¹ Qilin Sun¹ Felix Heide³ Wolfgang Heidrich^{1,2}
¹King Abdullah University of Science and Technology, Thuwal, Saudi Arabia
²The University of British Columbia, Vancouver, Canada
³Stanford University, Stanford, USA

Abstract

Depth-dependent defocus results in a limited depth-of-field in consumer-level cameras. Computational imaging provides alternative solutions to resolve all-in-focus images with the assistance of designed optics and algorithms. In this work, we extend the concept of focal sweep from refractive optics to diffractive optics, where we fuse multiple focal powers onto one single element. In contrast to state-of-the-art sweep models, ours can generate better-conditioned point spread function (PSF) distributions along the expected depth range with drastically shortened (40%) sweep distance. Further by encoding axially asymmetric PSFs subject to color channels, and then sharing sharp information across channels, we preserve details as well as color fidelity. We prototype two diffractive imaging systems that work in the monochromatic and RGB color domain. Experimental results indicate that the depth-of-field can be significantly extended with fewer artifacts remaining after the deconvolution.

1. Introduction

Extending depth-of-field (DOF) is an exciting research direction in computational imaging [32, 3], particularly for embedded cameras where a large numerical aperture (aka. a small f -number) is necessary to ensure high light throughput. Recent advances seek to design optics in combination with post-processing algorithms to either preserve more information or enable extra functionality by reducing the complexity of lenses.

Work on this problem ranges from capturing entire light field [23, 5] to engineering point spread function (PSF) shapes [6, 36, 19]. Using the prior knowledge on the mapping relation between kernel shapes and scene depths, one can recover all-in-focus images. Despite engineering PSF shapes on the pupil plane of a lens, another advance is to apply sweep type solutions such as spatial focal sweep or focal stack cameras [21, 11, 17].

The focal sweeps facilitate nearly *depth invariant* blur

kernel by capturing an integrated PSF over a time duration, and then apply a deconvolution step to remove the residual blur effect [34, 17]. Sweeping reduces calibration requirements of depth-variant PSFs in the capture. This strategy has been applied in not only imaging domain but projection display domain [12]. Despite much research, auxiliary mechanics is usually required to sweep either the optics or the sensor for a physical distance.

One common fact that has not been addressed by state-of-the-art sweep type cameras is that these systems rely on sweeping complex refractive optics. Planar optics, like diffractive optical elements (DOEs) or metasurface lenses, have recently been proven effective to shrink the camera lenses in both weight and thickness [24, 7]. Although this advantage is prominent for sweep configurations, a regular Fresnel lens still requires a considerably large sweep distance as its refractive counterpart.

Using DOEs as imaging lenses provides flexibility to create multiple foci with one single element [25]. Despite much research in optics on multi-focal lenses for ophthalmic and clinical applications [33, 15, 13], existing consumer-level cameras barely use this design. Theoretically by enabling multi-focal powers subject to depths, it is viable to shorten sweep distance as well as to achieve better conditioned integrating imaging (see Sec. 3.1).

In this work, we make the following contributions:

- We introduce a multi-focal sweep imaging system for extending depth-of-field from one aggregated image that incorporates optical design and post-capture image reconstruction.
- We propose a diffractive lens design that is fused with multiple focal powers subject to two aspects: expected depth-of-field, and three color channel fidelity. The better-conditioned kernel after sweeping integration leads to an efficient deconvolution to resolve all-in-focus images. Moreover, the color fidelity is preserved via enforcing cross-channel information sharing.
- We present two prototype lenses to validate the concept, with sweeping ultra-thin *tri-focal* and *novem-*

focal diffractive lenses. We test our deconvolution on different scenarios with large depth variance. The results exhibit visually pleasing quality, especially in terms of resolving all-in-focus images while preserving color fidelity and suppressing edging artifacts.

2. Related Work

Computational DOF extension. Capturing the entire light field can enable extending DOF or refocusing. Although lenslet-based light field cameras are available commercially [23, 5], the significant compromise of spatial resolution is problematic. Reviewing sweep-type solutions, focal sweep and focal stack strategies differ in that a focal sweep camera captures a single image while its focus is quickly swept over a depth range, and a focal stack camera captures a series of images at different focal settings subject to depths [37, 18]. The latter requires more complex capturing and processing procedure, so as to facilitate refocusing experience. In this work, we aim to extend DOF to resolve all-in-focus images.

An alternative approach is to leverage spectral focal dispersion along depth to replace the physical sweep motion [4]. Although the motion mechanics is removed, the resolved image quality relies significantly on the reflectance of the scene and the illumination spectra. That said, this approximation of depth invariant PSF behavior across color channels may result in artifacts where partial spectral information is absent in the scene. Furthermore, the DOF that can be extended is limited using chromatic aberration of regular refractive optics.

Image deconvolution. Recent advances in image deconvolution seek to include extra prior knowledge, like using a total variation (TV) prior [1], to restore high-frequency information. Cho *et al.* [2] proposed to match the gradient distribution for image restoration. Alternative non-convex regularization terms are intensively investigated [19, 16], empirically giving improved results at reasonable local optimum. This process can also be implemented in a blind manner [30]. Despite adding generic priors in the optimization, learning-based methods like convolutional neural network [26] have been reported.

Encoded diffractive imaging. Through PSF engineering, aberrations can be designed for easy computational removal. Early work of wave-front coding has proven to extend depth-of-field using a cubic phase design [6]. This work requires an extra focusing lens to provide focal power. The flexibility of DOE in modulating light has been highlighted recently as lensless computational sensors [29, 22] and as encoded lenses [24, 9]. The former designs attach DOEs in front of bare sensors to miniaturize form factor. The latter designs exhibit ultra-thin appearance in optics

volume and are successfully encoded in either spatial or spectral domain. However, the strong chromatic aberrations of DOEs directly limits their application in color imaging. Although Peng *et al.* [25] have reported a diffractive achromat that preserves color fidelity, it is still challenging to at the same time obtain high-resolution focusing over a large depth range. The bottleneck lies in the limited design freedom of the products that are viable with current fabrications. We yield the design bandwidth to resolve an image with reasonable spatial resolution within a large depth range or a large field-of-view (FOV). Then, we resolve color fidelity relying on computational imaging techniques.

Chromatic aberration correction. To remove color fringes on sharp edges resulted from different PSFs in channels, many low-level techniques have been applied in complex optical systems [14, 27]. Later on, a convex cross-channel prior is developed and efficiently solved [10]. The symmetry of the convolution kernel [28] and the geometric and visual priors [35] are investigated. Very recently, Sun *et al.* [31] investigated a blind deconvolution scheme that included cross-channel sharing in the fitting model. State-of-the-art models yield reasonably good results with chromatic aberration corrected. In this work, we revisit the cross-channel prior concept, while we don't assume a specific reference channel as in above work. In our design, all three channels contribute to the final deblurred image.

3. Optical Design

3.1. Multi-focal diffractive lens

We start by investigating the ability of a multi-focal lens on shortening the sweep distance of focal sweep imaging. Using geometry optics, the relationship among sweep distance s , foci number N , focal length difference Δf and fo-

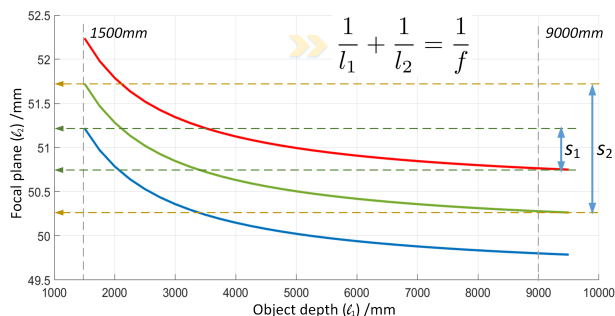


Figure 1: Comparison of focused distances subject to object distance and focal length under the assumption of thin lens model (the math derivation is given). The three color curves visualize the relations of using lenses with the focal length of 49.5mm, 50.0mm, 50.5mm, respectively. s_1 and s_2 represent the sweep distances needed for a tri-focal lens and a one-focal lens, respectively.

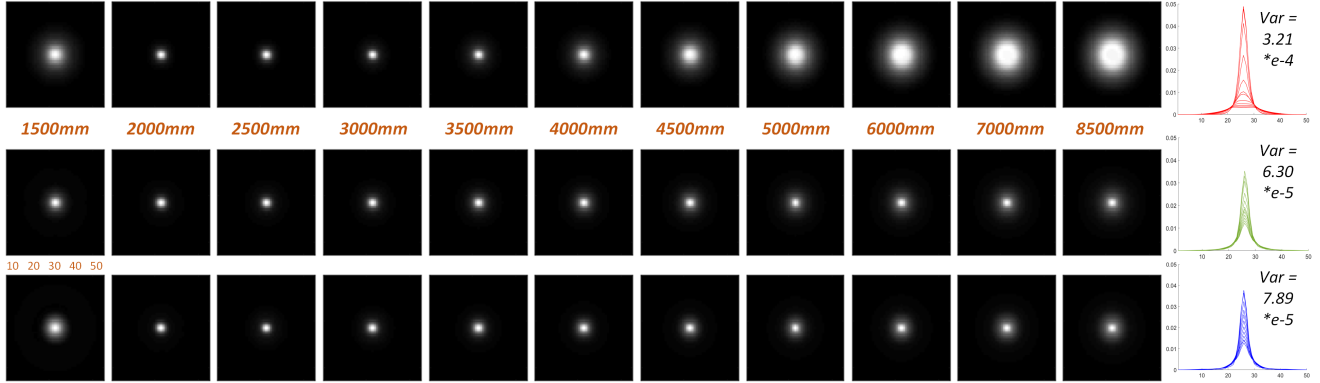


Figure 2: Comparison of synthetic PSF behavior of sweeping a regular Fresnel lens (top) and our tri-focal lens (center and bottom) subject to target depths. Notice that this design aims for monochromatic imaging that is integrated over a spectrum of 10nm FWHM. The axes of each subfigure represent the size with a pixel pitch of $5\mu\text{m}$. The normalized cross-sections (right-most) indicate that our multi-focal sweep designs exhibit less variance (quantized) regarding PSF distributions. We sacrifice the peak intensity at the central depth to minimize the variance of PSF distributions along full depth range.

cused depth range (on image end) l can be cast as follows:

$$\left[-\frac{l}{2}, \frac{l}{2}\right] \subseteq \bigcup_{n=0}^{N-1} \left[-\frac{s}{2} - \frac{2n - (N-1)}{2(N-1)} \Delta f, \frac{s}{2} - \frac{2n - (N-1)}{2(N-1)} \Delta f\right]. \quad (1)$$

Assume we consider a lens with a focal length of 50mm to cover the focused depth range (on object end) from 1.5m to 9m ($l = 1.4\text{mm}$), and the sweep distance is 0.5mm, then, the focal length difference Δf should be beyond 0.96mm and the foci number N should be at least 3. Subsequently, we can choose $\Delta f = 1\text{mm}$ and $N = 3$. This means the above requirements can be realized by using a tri-focal lens with the focal length of 49.5mm, 50mm, 50.5mm, respectively.

As shown in Fig. 1, it is clear that for a tri-focal lens, due to the approximately periodic distribution of focal planes along an expected depth range (the green, blue, and red curves), we only need to sweep image planes from 50.75mm to 51.25mm ($s = 0.5\text{mm}$) to cover the desirable focused depth range. However, for a lens with single focal length, we need to sweep the image plane from 50.3mm to 51.7mm ($s = l = 1.4\text{mm}$) to cover the same depth range from 1.5m to 9m (the green center curve). This matches the derivation of Eq. 1, indicating that the sweep distance can be drastically shortened by introducing multi-focal designs.

We note that the sweep distance derived above is the minimum sweep distance. In practice, we choose to use a relatively larger sweep distance, e.g. 0.8mm in the aforementioned scenario. This is reasonable considering the different defocus effect of each object plane within the range of the minimum sweep distance. The final kernel that is integrated over a sequence of more uniform depth PSFs leads to a better-conditioned deconvolution.

We generate the multi-focal lens by fusing multiple Fresnel lenses onto one single element. As mentioned above,

we design two lenses. First, we divide the aperture into three rings of equal area. Thus, the monochromatic design is a radial mixture of subregions screened from Fresnel lenses at the wavelength of 550nm for three different focal lengths, which we call *tri-focal lens*. Similarly, the RGB color design is an axially asymmetric mixture of three aforementioned monochromatic designs subject to three spectra, namely 640nm, 550nm, 460nm, which we call *novem-focal lens*. The graph fusion schemes and the microscope images of our prototype lenses are shown top of Fig. 3.

3.2. PSF behaviors

Figure 2 visualizes the synthetic PSF behaviors of a regular Fresnel lens and our tri-focal lens, swept along a distance of 0.8mm (top and center row) and 0.5mm (bottom row). We see that although none of its PSFs is highly focused, our tri-focal lens exhibits less variance in terms of the size of peripheral energy distribution over the full depth range. This more depth-invariant blur makes it possible to deconvolve the full image using only one calibrated PSF. We also note that PSFs become more depth-invariant when increasing the sweep distance slightly (center Fig. 2). This can be justified by the provided quantitative values as well. We will further explain our choice in the experiments.

Figure 3 visualizes the real PSF behaviors of our two multi-focal lenses swept over a distance of 0.5mm. Concerning our novem-focal lens (shown right Fig. 3), despite the relatively small variance regarding the size of peripheral energy distribution in different channels, the PSFs exhibit axially asymmetric shape with high-frequency components. As the high-frequency components vary in spatial distribution from channel to channel, it is possible to recover that with shared information from different channels.

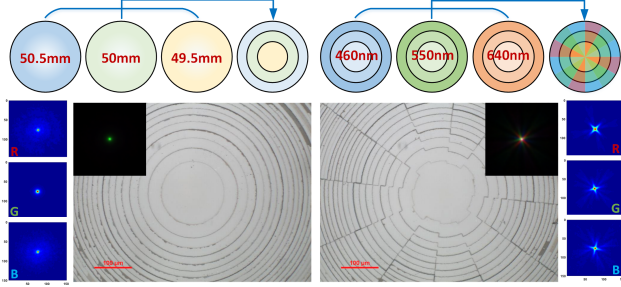


Figure 3: Diagrams of graph fusion schemes (top) and cropped microscope images of fabricated lenses as well as the experimental PSFs behavior of sweeping a tri-focal lens (bottom-left) and a novem-focal lens lens (bottom-right). This experiment aims for RGB color imaging that is integrated on a RGB Bayer sensor.

4. Image reconstruction

4.1. Sweeping image formation

The defocus effect can be formulated as a latent image convolved with a blur kernel. Then, we can write the recorded image in channel c in vector-matrix format as:

$$\mathbf{b}_c = \mathbf{K}_c \mathbf{i}_c + \mathbf{n}, \quad (2)$$

where for a channel c , \mathbf{b} , \mathbf{K} , \mathbf{i} , \mathbf{n} are the captured image, convolution matrix, sharp latent image and additive noise in the capture, respectively. Regarding a sweep imaging system with a diffractive lens, \mathbf{K}_c can be derived from the PSF P_c integrated over the depth range Δ and spectrum Λ as follows:

$$P_c(x, y) = \int_{\Lambda} \int_{\Delta} Q_c(\lambda) \cdot (P(x, y, z; \lambda)) d\lambda dz, \quad (3)$$

where $P(x, y, z; \lambda)$ is the spatial spectral variant PSF describing the aberrations of lens, which is a function of both spatial position (x, y, z) and spectral component λ . Q_c represents the sensor response, which can be reasonably assumed as the constant when used under narrowband scenario. As aforementioned, after sweeping integration the PSF P_c is approximately depth invariant.

4.2. Optimization method

To resolve all-in-focus images, we formulate the inverse problem of Eq. 2 as an optimization containing a least-squares data fitting term and a collection of priors that regularize the reconstruction.

Deconvolution on individual channels. Regarding the deconvolution of an individual channel, which is also the application scenario of monochromatic imaging, the prior

term $\Gamma(\mathbf{i}_c)$ is a total variation prior (i.e. l_1 -norm on gradients that are derived from multiplying a matrix \mathbf{D}). The optimization becomes as follows:

$$\mathbf{i}_c^d = \operatorname{argmin}_{\mathbf{i}_c} \frac{\mu_c}{2} \|\mathbf{b}_c - \mathbf{K}_c \mathbf{i}_c\|_2^2 + \|\mathbf{D} \mathbf{i}_c\|_1. \quad (4)$$

We can directly use the Split Bregman method [8] to efficiently solve Eq. 4. A trick is to assign a slightly larger weight of μ_c so as to yield the deconvolved result \mathbf{i}_c^d exhibiting sharp edges and features. The intermediate resolved images serve as references for cross-channel processing.

Cross-channel regularization. The cross-channel regularization follows closely the recent work [9]. This is realized by enforcing the gradient information to be consistent among different color channels. With respect to the color multi-focal sweep scenario, ours differs from state-of-the-art methods in that there is no specific sharp channel set as a reference. In our case, the images in three channels shall all serve as references, since the color PSF exhibits different behaviors. That said, although none of the three channels is sufficiently sharp before processing, each channel shall preserve the details of some sense to the recovery of images in others. The optimization then becomes as follows:

$$\mathbf{i}_c = \operatorname{argmin}_{\mathbf{i}_c} \frac{\alpha}{2} \|\mathbf{b}_c - \mathbf{K} \mathbf{i}_c\|_2^2 + \beta \|\mathbf{D} \mathbf{i}_c\|_1 + \sum_{m \neq 1} \gamma \|\mathbf{D} \mathbf{i}_c - \mathbf{D} \mathbf{i}_c^d\|_1, \quad (5)$$

where α, β, γ are tunable weights for each term.

Specially, Eq. 5 can be solved by introducing slack variables for the l_1 term and then using a similar solver scheme as in [25]. Although the deblurred images of each individual channel (Eq. 4) may suffer from sensor noise, most edges and features can be robustly recovered from the cross-channel information sharing. These roughly deblurred images \mathbf{i}_c^d are used as reference channel images in the cross-channel terms (Eq. 5) to iteratively recover the three channel images. We don't detail the algorithm here.

4.3. Efficiency and robustness analysis

We note that the cross-channel regularizer makes the optimization problem more complex and non-linear and the resolved results could be highly dependent on the quality of the reference channel. However, we manage to gain reasonable good results with a reasonable amount of tuning effort.

Using the color PSFs derived from two real prototype lenses, we have implemented simulations on a number of test images (BSDS500 dataset [20]). Extra 0.5% Gaussian noise is added. The comparison results are illustrated in Tab. 1. Additional visualization results are presented in Sec. 5.2. With respect to the tri-focal lens, we enforce cross-channel sharing only from the green channel image to the

other relatively blurred red and blue channel images. With respect to the novem-focal lens, we enforce cross-channel sharing between all three channel images. For the latter, the averaged run time for one image with the size of 1,384 by 1,036 pixels is around 7 seconds on Matlab IDE run on a laptop PC with 2.4GHz CPU and 16GB ram.

We have the two observations. First, enforcing cross-channel information sharing contributes to resolving higher quality images in both scenarios. Further, enabling graph fusion subject to colors in addition explores cross-channel information sharing to preserve higher color fidelity.

Table 1: Comparisons of synthetic image reconstruction with PSNR averaged over 100 dataset images. **1** indicates the tri-focal lens and **2** indicates the novem-focal lens.

| w/o. cross. 1 | w/. cross. 1 | w/o. cross. 2 | w/. cross. 2 |
|---------------|--------------|---------------|--------------|
| 20.392 | 23.299 | 23.523 | 24.625 |

5. Implementation and discussion

In this section, before presenting selected experimental results that validate the proposed approach, we start by introducing the parameters of our prototype lenses.

5.1. Prototype parameters

We have designed two types of multi-focal diffractive lenses, one for monochromatic imaging while the other for RGB color imaging. The aperture diameter is 8mm for both designs. The monochromatic one is designed at the central wavelength of 550nm and fused with 3 Fresnel lens patterns subject to focal lengths of 49.5mm, 50.0mm, 50.5mm. The color one is designed with fusing afore-designed monochromatic patterns subject to wavelengths of 640nm, 550nm, 460nm. Both lenses are attached in front of a PointGrey sensor (GS3-14S5C) that has the pixel pitch of $6.45\mu\text{m}$. The exposure time is 500ms for lab setting scenes and 650ms for office setting scenes, during when 0.5mm axial distance is swept. The experimental setup is illustrated in Fig. 4.

We fabricated our designed lenses by repeatedly applying photolithography and RIE techniques [25]. The substrate in our implementation is a 0.5mm Fused Silica wafer with an index of 1.459. We choose 16-phase-level microstructures to approximate the continuous surface profile. We use 4π phase modulation corresponding to $2.39\mu\text{m}$ etching depth on the wafer. The higher order diffraction benefits to yielding a short focal length (aka. small f -number) design with the practical feature size of state-of-the-art fabrication techniques.

5.2. Results

Simulation results of two standard images are presented in Fig. 5. From the zoomed-in insets, we observe that the axially asymmetric fusion design preserves higher color fi-

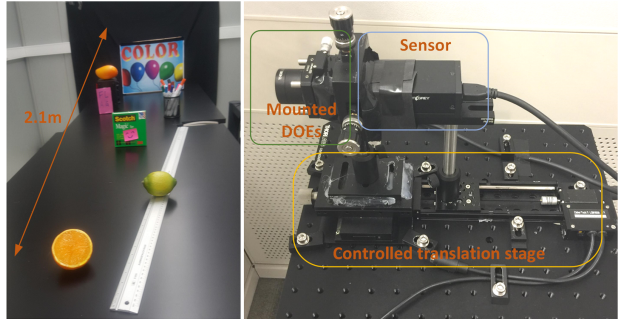


Figure 4: Photograph of our experimental setup. Left: a captured scene with a large depth range; Right: the prototype lenses are mounted on a holder while the sensor is mounted on a controlled translation stage.

delity than a regular symmetric multi-focal design, while its ability to distinguish fine details is slightly traded off.

The real world results are presented in Fig. 6 and in Fig. 7. The depth range is set from 1.5m to 3.5m for the lab setting scenes (shown left of Fig. 4) and set from 2m to 8m for the office setting scenes. In particular, since the first prototype aims for monochromatic imaging, the reconstructed results of green channel exhibit decent quality.

We first set the green channel as the reference and use a cross-channel prior to deconvolve the images. As shown bottom row of Fig. 6, although exhibiting reasonable spatial resolution, its color fidelity is quite low. This is because naive Fresnel lenses suffer from severe chromatic aberration. A regular cross-channel prior is not sufficiently robust to preserve both spatial frequency and color fidelity.

In contrast, the second prototype additionally favors axially asymmetric PSFs subject to three color channels. That said, we have a relatively high-intensity peak with high-frequency long tails of PSF in each channel such that in the deconvolution we can preserve color fidelity (shown in Fig. 7). However, limited by the data bandwidth of the DOE, we have to trade off the spatial resolution of some sense. The overall image quality is still visually acceptable. Again, this work aims for extending DOF rather than naively pursuing spatial resolution. From this perspective, despite the slight image contrast loss due to the fabrication and prototype issues, our multi-focal lenses outperform off-the-shelf products, as shown in Fig. 8. To achieve a competitive DOF performance, one need to drastically shrink down the aperture to at least a f -number 12, which requires much longer exposure in practice.

5.3. Discussions

On optics end, current fusion scheme of multiple foci is derived in a heuristic manner and shows only two effective designs. The optimal spatial distribution of PSFs may vary. Designing fusion schemes in an intelligent way remains an

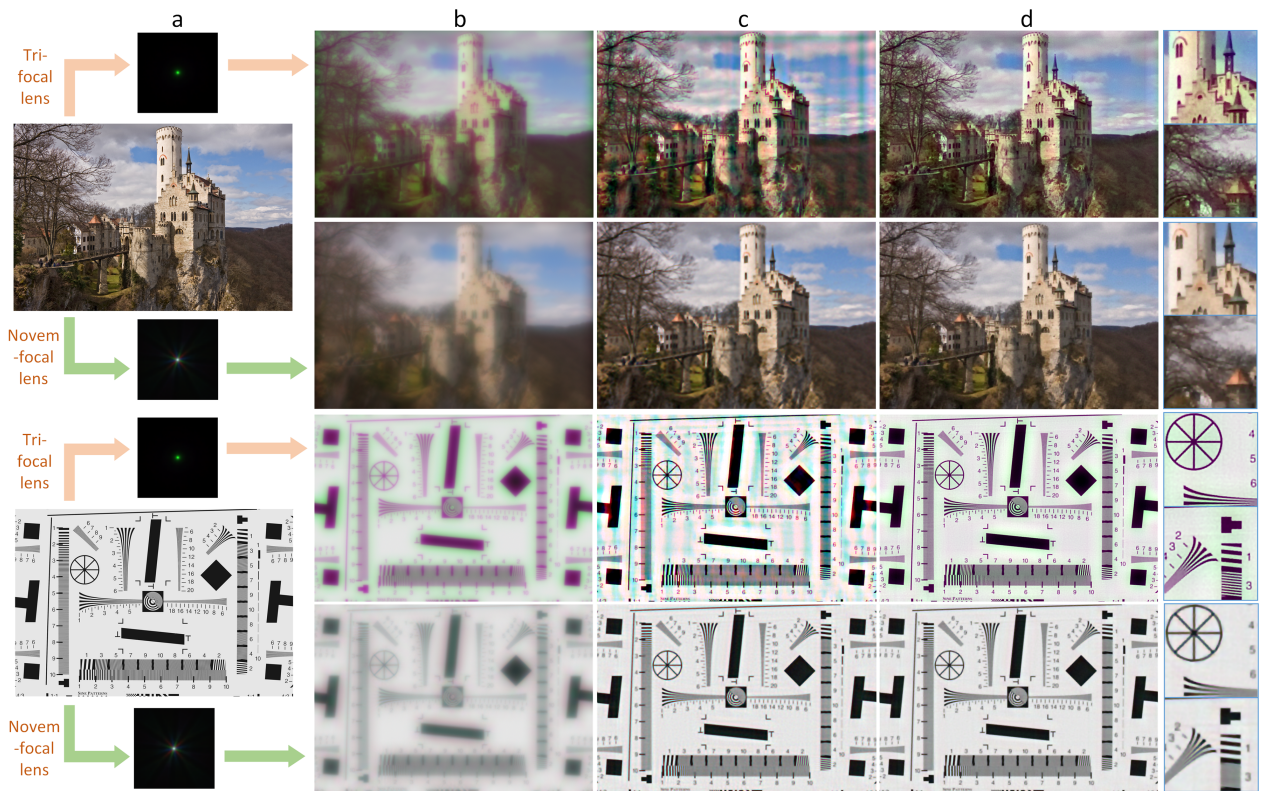


Figure 5: Simulation results: (a) ground truth inputs and kernels; (b) degraded images blurred by corresponding kernels; (c) reconstruction results using TV-based deconvolution on individual channels; (d) reconstruction results using deconvolution with TV and cross-channel regularization. The two color PSFs used to degrade the images are calibrated from the two prototype lenses under white point light source illumination. In addition to the background noise in the calibrated PSFs (see insets in Fig. 3), 0.5% white noise is added.



Figure 6: Cropped regions of real world results. Top: degraded inputs; Bottom: reconstruction results using deconvolution with TV and cross-channel regularizations. For experimental convenience, we capture a depth range from 1.5m to 3.5m for the left two scenes and from 2m to 8m for the right scene with a sweep distance of 0.5mm. We use the single calibrated PSF shown in Fig. 3 to deconvolve all images.

open but interesting direction. We anticipate learning strategies, like look-up table or dictionary search, can be used to

guide the design.

Remaining artifacts like low image contrast and residual

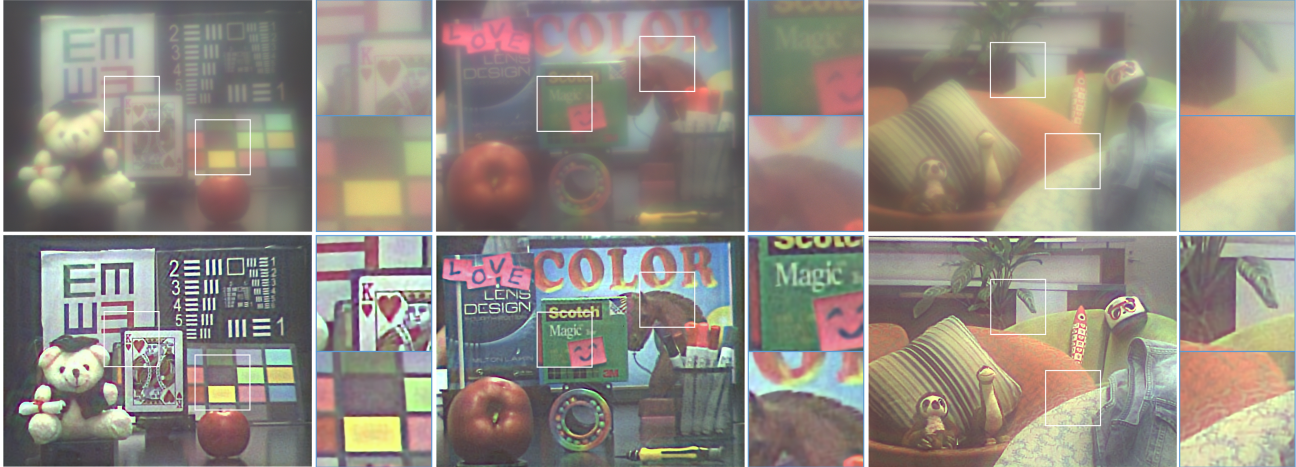


Figure 7: Cropped regions of real world results. Top: degraded inputs; Bottom: reconstruction results using deconvolution with TV and cross-channel regularizations. We use the same experimental setting as in Fig. 6.

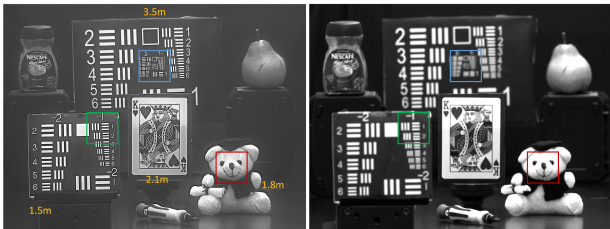


Figure 8: DOF comparison between our tri-focal lens (left) and a standard EF50 (Canon) refractive lens (right), both with a f -number 6.25. The scene depth range is 1.5m to 3.5m, highlighted by different color rectangles. We here extract the green channel for a fair comparison.

blur are due to several engineering factors. Careful readers may observe from the results that a slight shift (2-pixel level) occurs when sweeping the lens. This is mainly because our sweeping axis is not strictly perpendicular to the sensor plane. The customized lens holder and cover may introduce ambient light that amplifies the noise. We also note that metamerism issues exist since the scope is not aiming for full spectrum, thus slight color artifacts may remain when used under white light illumination.

In addition, current DOEs with 16-level structure still suffer from a non-trivial diffraction efficiency loss, especially for high diffraction order designs, that is observed as low image contrast and additional blur. Due to the inherent limitation of feature size, it is challenging to create a diffractive lens with a high numerical aperture (aka. small f -number). This fabrication constraint can be overcome by more advanced methods like nano-imprinting or grayscale photolithography.

On reconstruction end, the cross-channel regularization can be further exploited. We anticipate there exists a better

strategy to define reference channels rather than enforcing current two-step deconvolution scheme. Additional denoising solver can be added to obtain better visualization.

On application end, the narrowband design is promising in surveillance scenarios where a large FOV and a large DOF are strongly acknowledged. In addition, depth sensors with active illumination are excellent platforms where our multi-focal lenses can be incorporated. Active illumination ensures that fusing a few wavelengths is reasonable so as to yield great design freedom to extend DOF.

6. Conclusion

We have proposed a computational imaging approach that jointly considers sweeping diffractive design and image reconstruction algorithms, and demonstrated the practicality of extending depth-of-field with compact lenses. Benefiting from the design flexibility of diffractive optics, the proposed design significantly shortens the required sweep distance meanwhile exhibits a better conditioned depth-invariant kernel behavior.

Moreover, color fidelity is preserved by fusing spectral variant PSF behaviors in the diffractive lens design and enforcing cross-channel regularization in the deconvolution. We have validated the effectiveness and robustness of our method with a variety of captured scenes. Although current experimental results suffer from the problems of slight blurry and low contrast that can be resolved via a reasonable amount of engineering effort, our approach shall be an effective solution to extend depth-of-field especially in situations where thin and lightweight optics is expected.

Acknowledgement

This work is supported by the KAUST baseline funding. The authors thank Gordon Wetzstein and Lei Xiao for fruit-

ful discussion.

References

- [1] S. H. Chan, R. Khoshabeh, K. B. Gibson, P. E. Gill, and T. Q. Nguyen. An augmented lagrangian method for total variation video restoration. *IEEE TIP*, 20(11):3097–3111, 2011. [2](#)
- [2] T. S. Cho, C. L. Zitnick, N. Joshi, S. B. Kang, R. Szeliski, and W. T. Freeman. Image restoration by matching gradient distributions. *IEEE TPAMI*, 34(4):683–694, 2012. [2](#)
- [3] O. Cossairt, M. Gupta, and S. K. Nayar. When does computational imaging improve performance? *IEEE TIP*, 22(2):447–458, 2013. [1](#)
- [4] O. Cossairt and S. Nayar. Spectral focal sweep: Extended depth of field from chromatic aberrations. In *Proc. ICCP*, pages 1–8, 2010. [2](#)
- [5] D. G. Dansereau, O. Pizarro, and S. B. Williams. Linear volumetric focus for light field cameras. *ACM TOG*, 34(2):15–1, 2015. [1, 2](#)
- [6] E. R. Dowski and W. T. Cathey. Extended depth of field through wave-front coding. *Applied optics*, 34(11):1859–1866, 1995. [1, 2](#)
- [7] P. Genevet, F. Capasso, F. Aieta, M. Khorasaninejad, and R. Devlin. Recent advances in planar optics: from plasmonic to dielectric metasurfaces. *Optica*, 4(1):139–152, 2017. [1](#)
- [8] T. Goldstein and S. Osher. The split bregman method for l1-regularized problems. *SIIMS*, 2(2):323–343, 2009. [4](#)
- [9] F. Heide, Q. Fu, Y. Peng, and W. Heidrich. Encoded diffractive optics for full-spectrum computational imaging. *Scientific Reports*, 6, 2016. [2, 4](#)
- [10] F. Heide, M. Rouf, M. B. Hullin, B. Labitzke, W. Heidrich, and A. Kolb. High-quality computational imaging through simple lenses. *ACM TOG*, 32(5):149, 2013. [2](#)
- [11] S. Honnunar, J. Holloway, A. K. Pediredla, A. Veeraraghavan, and K. Mitra. Focal-sweep for large aperture time-of-flight cameras. In *Proc. ICIP*, 2016. [1](#)
- [12] D. Iwai, S. Mihara, and K. Sato. Extended depth-of-field projector by fast focal sweep projection. *IEEE TVCG*, 21(4):462–470, 2015. [1](#)
- [13] J. C. Javitt and R. F. Steinert. Cataract extraction with multifocal intraocular lens implantation: a multinational clinical trial evaluating clinical, functional, and quality-of-life outcomes. *Ophthalmology*, 107(11):2040–2048, 2000. [1](#)
- [14] S. B. Kang. Automatic removal of chromatic aberration from a single image. In *Proc. CVPR*, pages 1–8, 2007. [2](#)
- [15] R. H. Keates, J. L. Pearce, and R. T. Schneider. Clinical results of the multifocal lens. *Journal of Cataract & Refractive Surgery*, 13(5):557–560, 1987. [1](#)
- [16] D. Krishnan and R. Fergus. Fast image deconvolution using hyper-laplacian priors. In *Proc. ANIPS*, pages 1033–1041, 2009. [2](#)
- [17] S. Kuthirummal, H. Nagahara, C. Zhou, and S. K. Nayar. Flexible depth of field photography. *IEEE TPAMI*, 33(1):58–71, 2011. [1](#)
- [18] M. Lee and Y.-W. Tai. Robust all-in-focus super-resolution for focal stack photography. *IEEE TIP*, 25(4):1887–1897, 2016. [2](#)
- [19] A. Levin, R. Fergus, F. Durand, and W. T. Freeman. Image and depth from a conventional camera with a coded aperture. *ACM TOG*, 26(3):70, 2007. [1, 2](#)
- [20] D. Martin, C. Fowlkes, D. Tal, and J. Malik. A database of human segmented natural images and its application to evaluating segmentation algorithms and measuring ecological statistics. In *Proc. ICCV*, pages 416–423. IEEE, 2001. [4](#)
- [21] D. Miao, O. Cossairt, and S. K. Nayar. Focal sweep videography with deformable optics. In *Proc. ICCP*, pages 1–8, 2013. [1](#)
- [22] M. Monjur, L. Spinoulas, P. R. Gill, and D. G. Stork. Ultra-miniature, computationally efficient diffractive visual-bar-position sensor. In *Proc. ICSTA*, pages 24–29, 2015. [2](#)
- [23] R. Ng, M. Levoy, M. Brédif, G. Duval, M. Horowitz, and P. Hanrahan. Light field photography with a hand-held plenoptic camera. *CSTR*, 2(11):1–11, 2005. [1, 2](#)
- [24] Y. Peng, Q. Fu, H. Amata, S. Su, F. Heide, and W. Heidrich. Computational imaging using lightweight diffractive-refractive optics. *Optics express*, 23(24):31393–31407, 2015. [1, 2](#)
- [25] Y. Peng, Q. Fu, F. Heide, and W. Heidrich. The diffractive achromat full spectrum computational imaging with diffractive optics. *ACM TOG*, 35(4):31, 2016. [1, 2, 4, 5](#)
- [26] C. J. Schuler, H. Christopher Burger, S. Harmeling, and B. Scholkopf. A machine learning approach for non-blind image deconvolution. In *Proc. CVPR*, 2013. [2](#)
- [27] C. J. Schuler, M. Hirsch, S. Harmeling, and B. Scholkopf. Non-stationary correction of optical aberrations. In *Proc. ICCV*, pages 659–666, 2011. [2](#)
- [28] C. J. Schuler, M. Hirsch, S. Harmeling, and B. Scholkopf. Blind correction of optical aberrations. In *Proc. ECCV*, pages 187–200, 2012. [2](#)
- [29] D. G. Stork and P. R. Gill. Lensless ultra-miniature cmos computational imagers and sensors. *Proc. SENSORCOMM*, pages 186–190, 2013. [2](#)
- [30] L. Sun, S. Cho, J. Wang, and J. Hays. Edge-based blur kernel estimation using patch priors. In *Proc. ICCP*, pages 1–8, 2013. [2](#)
- [31] T. Sun, Y. Peng, and W. Heidrich. Revisiting cross-channel information transfer for chromatic aberration correction. In *Proc. CVPR*, pages 3248–3256, 2017. [2](#)
- [32] M. W. Tao, S. Hadap, J. Malik, and R. Ramamoorthi. Depth from combining defocus and correspondence using light-field cameras. In *Proc. ICCV*, pages 673–680, 2013. [1](#)
- [33] H. A. Weeber. Diffractive multifocal lens having radially varying light distribution, 2011. US Patent 7,871,162. [1](#)
- [34] R. Yokoya and S. K. Nayar. Extended depth of field catadioptric imaging using focal sweep. In *Proc. ICCV*, pages 3505–3513, 2015. [1](#)
- [35] T. Yue, J. Suo, J. Wang, X. Cao, and Q. Dai. Blind optical aberration correction by exploring geometric and visual priors. In *Proc. CVPR*, 2015. [2](#)
- [36] C. Zhou, S. Lin, and S. Nayar. Coded aperture pairs for depth from defocus. In *Proc. ICCV*, pages 325–332, 2009. [1](#)
- [37] C. Zhou, D. Miao, and S. K. Nayar. Focal sweep camera for space-time refocusing. *Technical Report, Department of Computer Science*, 2012. [2](#)